論文 / 著書情報
Article / Book Information

Title	Effects of internal erosion on parameters of subloading Cam-clay model
Authors	Gang Wang, Kazuki Horikoshi, Akihiro Takahashi
Citation	Geotechnical and Geological Engineering, Vol. 38, issue 2, pp. 1323-1335
Pub. date	2020, 4
Copyright	This version of the article has been accepted for publication, after peer review (when applicable) and is subject to Springer Nature ' s AM terms of use, but is not the Version of Record and does not reflect post-acceptance improvements, or any corrections. The Version of Record is available online at: http://dx.doi.org/10.1007/s10706-019-01093-8

Effects of internal erosion on parameters of subloading Cam-clay model

Wang Gang
Graduate student, Department of Civil and Environmental Engineering, Tokyo Institute of Technology, Tokyo, Japan

Kazuki Horikoshi
Assistant professor, Department of Civil and Environmental Engineering, Tokyo Institute of Technology, Tokyo, Japan

Akihiro Takahashi*
Professor, Department of Civil and Environmental Engineering, Tokyo Institute of Technology, Tokyo, Japan

* Corresponding author
2-12-1-M1-3 Oh-okayama, Meguro, Tokyo 152-8552, Japan
Tel: +81-3-5734-2593, E-mail: takahashi.a.al@m.titech.ac.jp

Abstract

Internal erosion is widely detected in both natural deposits and earthen structures and potentially causes severe disasters. Suffusion is one of the modes of internal erosion in which fine particles in the soil are washed out along with water flow through pores formed by coarse particles. Mechanical consequences of internal erosion, specifically, suffusion, are not well investigated in term of constitutive modelling. Also, most of the present constitutive models concerning suffusion are validated by DEM simulations, not by actual soil response observed in soil tests. In this paper, triaxial seepage tests followed by drained compression on soil with 35% initial fines content under 50 kPa, 100 kPa and 200 kPa mean stresses are studied to investigate the applicability of the existing soil model to internally eroded soils. The subloading Cam-clay model is used to simulate the mechanical behaviour of eroded soils. After confirming that the model can capture key features of uneroded specimens, the evolution of model parameters with erosion is examined by back analysis of the eroded specimens. From the simulation on the eroded specimens, evolutions of the slope of normal compression line and initial stress ratio with erosion are quantified. The changes of model parameters with erosion provide a useful reference for investigating the mechanical behaviour of granular materials subjected to suffusion.

Keyword: internal erosion; suffusion, granular materials; model parameters; subloading Cam-clay model

Geotechnical and Geological Engineering, 38(2), 1323-1335, 2020

Original URL:

https://doi.org/10.1007/s10706-019-01093-8

1. Introduction

Internal erosion happens under the seepage flow, which includes concentrated leak erosion, contact erosion, backward erosion, and suffusion (Fry, 2012; Fell and Fry, 2013). Among them, suffusion describes the phenomenon that finer particles are eroded through the voids between the coarse particles by seepage flow. Fannin et al. (2014) subdivided the suffusion into two; suffosion and suffusion. Suffosion indicates the phenomenon in which collapse of soil structure happens after the loss of soil mass, while suffusion is a phenomenon where the soil structure and volume remain unchanged with the gradual loss of soil particles under seepage forces. This type of internal erosion is widely observed both in natural deposits and in earthen structures. For instance, erosion of fine fraction, induced by water table change in downtown Milan, was reported and it caused the settlements of foundations (Cividini et al. 2009). Two sinkholes appeared in WAC Bennett Dam due to the transportation of fine fraction toward downstream for many years (Muir Wood & Maeda 2008) and Wilson et al. (2018) noted that levee and dam failures occurred due to continuing soil erosion by the subsurface flow. In this paper, suffusion (without distinction to suffosion) is taken up and the term "internal erosion" is used to describe suffusion type of erosion.

Study on constitutive models plays a significant role in understanding the mechanical behaviour of internally eroded soils. Since the loss of fine particles changes the particle size distribution, Muir Wood et al (2010) proposed the grading state index. This index denoted the ratio of current grading area and limiting grading area on the particle size distribution curves, which could be incorporated into the formulation of state parameter. In their study, mechanical behaviour of eroded soils was simulated by Severn-Trent sand model with considering the effect of grading change and was validated by DEM analysis. Hicher (2013) proposed a micromechanical method to simulate the stress-strain relationship of eroded granular materials. Similar mechanical trends of granular soils subjected to internal erosion could be obtained by both proposed approach and DEM simulation, and a phenomenon called diffuse failure was observed in the eroded soils through both simulation results and experimental evidence. Considering four effects of internal erosion, i.e., loosening, force network relaxation, force network damage and critical state change, Wang and Li (2015) investigated the impacts of erosion mass percentage, the current mean stress and deviatoric stress on these effects. In their study, in the light of DEM simulation, incremental equations of void ratio, mean stress, deviatoric stress, volumetric strain, and specific volume were established with independent variables such as erosion mass percentage, mean stress and deviatoric stress. Their theoretical results calculated from state-based constitutive model considering four effects agreed well with the DEM simulation results.

Recently, many experimental investigations have been carried out on the stress-strain behaviour of internally eroded soils (Chang et al. 2014; Ke & Takahashi 2014; Ke & Takahashi 2015; Ouyang & Takahashi 2015; Li et al. 2017; Mehdizadeh et al. 2017). However, up to now, most of the constitutive models for erosion considered particle removal of granular soils and were validated by DEM results and limited number of constitutive models have been validated by results from laboratory experiments. There remains a need for further investigations on the variations of model parameters caused by internal erosion with refer to experimental evidences. In this paper, firstly, seepage-induced erosion tests under different mean stresses are described. These tests show the erosion-induced variations of basic properties such as particle size distribution, fines content, and void ratio. Then, the mechanical behaviour of uneroded and eroded soils under drained triaxial compression tests are compared. Secondly, after confirming the simulation capability of the subloading Cam-clay model for uneroded specimens, the mechanical response of eroded soils is simulated using the same model. Finally, the evolution of key parameters with erosion is examined and analysed.

2. Experimental Investigations

Ke and Takahashi (2015) performed triaxial seepage tests to understand the mechanical behaviour of soils subjected to internal erosion. The apparatus consists of three units; constant-flow-rate control unit, triaxial unit, and eroded soil collection unit (Ke & Takahashi 2014). Independent control of hydraulic condition and stress state of soil samples is available in this apparatus. This apparatus allows measuring cumulative eroded soil mass, axial load, axial strain, radial strain, and pore water pressure.

The specimens were mixtures of Silica No.3 (coarse particles) and Silica No.8 (fine particles). The properties of these silica sands used are summarised in Table 1. For both uneroded and eroded specimens, initial fines content (Silica No.8 is regarded as fines for simplicity and fines content in this paper is defined as the mass ratio of Silica No.8 to the total soil) was 35%; confining pressures were 50kPa, 100kPa, and 200kPa. The downward flow was applied to the specimens by the constant-flow-rate control unit. The inflow rate of 310 mL/min was selected, which could cause significant fines loss. The whole inflow process was divided into three stages to avoid the collapse of structures formed by particles aa shown in Fig. 1. In stage 1, flow rate increment was 10 (mL/min)/min for 10 minutes until the flow rate reached 100 mL/min. In stage 2, the flow rate increment was 50 (mL/min)/min for 4 minutes until the flow rate reached 300 mL/min. Finally, in stage 3, the flow rate was increased to the target value (310 mL/min) and the flow rate was kept constant for at least three hours.

During the seepage tests, downward discharge effluent along with fine particles flowed into the eroded soil collection unit through a pipe. The cumulative fine particles remained in the light tray were continuously measured by a high sensitive waterproofed load cell. Figure 2 illustrates post-erosion grading curves under different mean stresses (50kPa, 100kPa, 200kPa). Comparing with the initial grading curve, post-erosion grading curves shift downward clearly in the fine fraction. Amount of this shifting of grading curves depends on the applied mean stress. Uniformity coefficient and curvature coefficient for the uneroded and eroded specimens are calculated and summarised in Table 2. Both curvature coefficient and uniformity coefficient varied dramatically due to erosion.

Figure 3 presents erosion-induced changes of fines content for the different initial mean effective stresses. For 50kPa initial mean effective stress, the specimen experienced the largest fines content loss, and the fines content decreased from 35% to 13.1%. With the larger initial mean effective stress, the fines loss was less compared to the case with 50kPa initial mean effective stress as shown in the figure. Bendahmane et al. (2008) observed that the increase in the confining pressure would result in decrease in the maximum erosion rate. The larger initial mean effective stress may have caused the tighter interlocking between particles, which made it more difficult for small particles to migrate under seepage flow. The same tendency can be seen in the tests reported here. Before the seepage test, the void ratio was almost the same for all the cases (cf. Fig. 4). The internal erosion made the void ratio larger, especially in the case with 50kPa initial mean effective stress and the void ratio increased from 0.55 to 1.01. After the seepage tests, the measured volumetric strain was ranged from 2.5% to 4%.

A series of drained triaxial tests were carried out for both uneroded and eroded specimens under 50kPa, 100kPa and 200kPa confining stresses (ASTM D7181-11 2012). These tests were strain-controlled with the axial strain rate of 0.1%/min. Figure 5a shows the changes of deviatoric stress with axial strain. For the same initial confining pressure, deviatoric stress of specimen with erosion is smaller than that without erosion at the relatively large axial strain level. However, deviatoric stress of specimen with erosion is larger than that without erosion when the axial strain is small (less than 1%, see Fig. 5b). Because the new arrangement of fine particles after erosion may have strengthened the specimens, the stiffness of the eroded specimens are larger than that of the uneroded specimen. However, the new arrangement collapsed with straining, resulting in the smaller secant stiffness at the larger strain level. As for the volumetric strain change, no large difference can be seen among the cases, but the volume change for the eroded specimens are slightly smaller than that of the uneroded one (Fig. 5c).

3. Constitutive model

3.1 Model description

125 Hashiguchi (1989) proposed the concept of subloading surface, which can describe the plastic deformation of a
126 material even inside the normal yield surface. The current stress state point is always on the subloading surface
127 and the normal yield surface can expand or contract with the movement of the subloading surface. The subloading
128 surface is geometrically similar to Cam-clay (normal) yield surface as shown in Fig. 6.

129 In the *p*-*q* space, the yield function of the normal yield surface can be expressed as

130 $$f = C_p \ln \frac{p^*}{p_N} + D\frac{q^*}{p^*} = 0 \tag{1}$$

131 where $C_p = \frac{\lambda - \kappa}{1 + e_0}$, $D = \frac{C_p}{M}$ (Zhu et al. 2013), λ is the slope of normal compression line in *e*-ln *p* space, κ is the
132 slope of swelling line in *e*-ln *p* space. *p* is mean effective stress (all mean stresses *p* in this paper represent mean
133 effective stresses) and *q* is deviatoric stress. *M* is the slope of the critical state line in *p*-*q* space, e_0 is the initial
134 void ratio. p_S and p_N are intersection points of the subloading and normal yield surfaces and mean effective stress
135 axis. p^* and q^* are mean effective stress and deviatoric stress on the normal yield surface, respectively.
136 The current stress state (*p*, *q*) is on the subloading surface. By considering the concept of subloading surface, Eq.
137 (1) can be rewritten as:

138 $$f = C_p \left[\ln \frac{p}{p_0} - \left(\ln \frac{p_N}{p_0} - \ln \frac{p_N}{p_s} \right) \right] + D\frac{q}{p} = 0 \tag{2}$$

139 where p_0 is the reference pressure (98kPa). The plastic volumetric strain caused by isotropic compression from p_0
140 to p_N, is expressed as

141 $$\varepsilon_v^p = C_p \ln \frac{p_N}{p_0} \tag{3}$$

142 where $R = \frac{p_S}{p_N}$ is stress ratio that corresponds to the size ratio of subloading surface to normal yield surface, and
143 is also the reciprocal of over consolidation ratio. By using Eq. (3), the subloading surface can be written as

144 $$f = C_p \ln \frac{p}{p_0} - \varepsilon_v^p - C_p \ln R + D\frac{q}{p} = 0 . \tag{4}$$

145 Since the current stress state point has to be on the subloading surface all the time, the following consistency
146 conditions has to be satisfied:

147 $$df = \frac{\partial f}{\partial p}dp + \frac{\partial f}{\partial q}dq + \frac{\partial f}{\partial R}dR - \frac{1}{C_p}d\varepsilon_v^p = 0\,. \tag{5}$$

148 When associated flow rule is adopted to the subloading surface, the plastic strain increments can be calculated as

149 $$d\varepsilon_v^p = \Lambda\frac{\partial f}{\partial p}\ ,\ d\varepsilon_q^p = \Lambda\frac{\partial f}{\partial q} \tag{6}$$

150 where Λ is the plastic multiplier (non-negative). The evolution rule of R is as follows (Hashiguchi, 1989).

151 $$dR = Ud\varepsilon_q^p \tag{7}$$

152 where $U = -m_R \ln R \cdot \frac{1}{D}$, and m_R is a material constant.

153 By substituting Eq. (6), (7) into (5), Λ can be obtained：

154 $$\Lambda = \frac{\frac{\partial f}{\partial p}dp + \frac{\partial f}{\partial q}dq}{\frac{1}{R}\frac{\partial f}{\partial q} + \frac{1}{C_p}\frac{\partial f}{\partial p}}\,. \tag{8}$$

155 From this plastic multiplier, the following constitutive equation can be obtained:

156 $$\begin{pmatrix} dp \\ dq \end{pmatrix} = \mathbf{D}_{ep}\begin{pmatrix} d\varepsilon_v \\ d\varepsilon_q \end{pmatrix}. \tag{9}$$

157 The elasto-plastic stiffness matrix in Eq. (9) can be written as,

158 $$\mathbf{D}_{ep} = \mathbf{D}_e - \frac{\mathbf{D}_e\partial\mathbf{f}\partial\mathbf{f}^T\mathbf{D}_e}{\partial\mathbf{f}^T\mathbf{D}_e\partial\mathbf{f} + H} \tag{10}$$

159 where $\mathbf{D}_e = \begin{bmatrix} K & 0 \\ 0 & 3G \end{bmatrix}$, $\partial\mathbf{f}^T = \begin{Bmatrix} \frac{\partial f}{\partial p} & \frac{\partial f}{\partial q} \end{Bmatrix}$, K is bulk modulus and G is shear modulus. G and K can be

160 expressed by the following equations (Richart et al. 1970):

161 $$G = G_0\frac{(2.97-e)^2}{1+e}\sqrt{pp_a} \qquad K = G\frac{2(1+\nu)}{3(1-2\nu)} \tag{11}$$

162 where G_0 is initial shear modulus, e is void ratio, p_a is the atmosphere pressure (98kPa), ν is Poisson's ratio.

163 ε_v^p and R are hardening parameters and the hardening function can be written as

$$H = \frac{1}{R}\frac{\partial f}{\partial q} + \frac{1}{C_p}\frac{\partial f}{\partial p}. \quad (12)$$

3.2 Model validation for uneroded soil

Key parameters in the model above are λ, κ, M, e_0, and initial value of R. Isotropic compression test has been conducted on uneroded specimens with 35% initial fines content. The specific volume variation with mean effective stress is plotted in Fig. 7. As the normal compression line (NCL) is not straight along with the mean effective stress, it is divided into two distinct regions. The first one is the elastic rebound curve under the low stress while the other is elasto-plastic linear compression curve under the higher stress (Gregory et al. 2006). Since the greater part of the normal compression curve is approximately straight for the soil used, the slope of the normal compression line is expressed as λ ($= \frac{e_1 - e_2}{\ln(p_2 / p_1)}$). The value of λ can be estimated by the fitting of the higher-pressure part of the compression curve. Since the swelling line (SL) is a straight line, the slope of the swelling line (κ) can be directly fitted. As the estimated preconsolidation pressure (p_c) is 70 kPa, the initial stress ratio (R) for the case with 50kPa confining pressure is estimated as 0.71 (see Fig. 7) and is set 1.0 for the other cases. Poisson's ratio is assumed 0.2 for all the tests.

When deviatoric stress of a specimen shows constant value with increasing the axial strain and keeping volume constant, the soil can be regarded as in the critical state and M (stress ratio at the critical state) can be determined from the effective stress paths (Fig. 8). The stress-strain curves (cf. Fig. 5) show that the deviatoric stress increases gradually and reaches a peak value with the axial strain. However, as the experiments were terminated at the axial strain from 12% to 18%, the samples have not reached the critical state. To estimate the deviatoric stress at the critical state, the fitting with a hyperbolic function was proposed (Ferreia & Bica 2006),

$$q = \frac{\varepsilon_a}{a_0 + b_0 \varepsilon_a} \quad (13)$$

where a_0 and b_0 are constants, which can be determined by the fitting. $1/b_0$ is regarded as the deviatoric stress at the critical state. For the drained triaxial compression tests, the slope of the stress path is three in the $p - q$ space (Fig. 9). The slope of the critical state line (M) can be estimated by the parameter b_0 above. For triaxial compression tests, the angle of shearing resistance (φ) can be obtained from Eq. (14),

$$M = \frac{6\sin\varphi}{3 - \sin\varphi} \quad (14)$$

189 Based on the back analysis, we estimate the parameter for the evolution of R as m_R = 0.1 and G_0 is estimated as
190 100 MPa. Parameters used in the simulations are summarised in Table 3. Simulation results are plotted in Fig. 10
191 (Sim. represents simulation results and Exp. represents experiment results). From Fig. 10 it can be said that the
192 subloading Cam-clay model can reasonably capture the features of uneroded specimens under drained triaxial
193 compression tests. Thus, it is decided to use the subloading Cam-clay model for simulation of post-erosion
194 specimens.

195 4. Results and discussions

196 4.1 Fines content and particle packing

197 Depending on the function of fines in binary packing, the states of soils with different fines contents are classified
198 into either coarse particles dominated or fine particles dominated (Lade et al. 1998). In the coarse particles
199 dominated case, coarse particles bear most of the forces and both maximum void ratio (e_{max}) and minimum void
200 ratio (e_{min}) decreases with increase of the fines content (Andrianatrehina et al. 2016). When the voids of coarse
201 particles are full of fine particles, the transitional fines content (FC_t) is reached (Yang et al. 2005). In the condition
202 of fine particles dominated, fines isolate coarse particles and constitute a network, which determines the
203 mechanical behaviour of soils. Zuo and Baudet (2015) summarised many methods for the determination of FC_t,
204 including the minimum value of e_{max} and e_{min}, the minimum value of vertical intercepts of normal compression
205 line or critical state line at a certain mean stress in the specific volume – the logarithm of the mean effective stress
206 space, the minimum number of cycles to liquefaction and so on. In this paper, FC_t is determined from the minimum
207 value of e_{max} and e_{min}. Figure 11 presents variations of maximum void ratio and minimum void ratio against fines
208 contents of the binary silica sands. The FC_t is determined to be 35%, at which both maximum and minimum void
209 ratios show a trough. When fines content is smaller than FC_t, coarse particles dominate the mechanical behaviour
210 of binary mixed soils. The fines merely fill the void space formed by the coarse particles when the fines content
211 is between zero and FC_t. When the fines content is larger than FC_t, fine particles play a greater role in the soil
212 structure.

213 4.2 Influence of fines content on the angle of shearing resistance

214 Table 4 summarises the previous studies on the variations of fines contents on the soil shear strength. It is apparent
215 that there are both positive correlation and negative correlation between fines content and shear strength, which
216 means the shear strength or angle of the shear resistance is also affected by other factors, such as void ratio,
217 mineral composition, particle shape, particle size distribution, the method of specimen preparation and so on. For
218 Samples 6 and 7, shearing tests on eroded soils were also conducted. They were prepared by binary poorly graded

sands, after a certain time period of seepage flow, both angles of shearing resistance at peak and at critical state became smaller with the loss of fines.

The initial fines content (FC_0) is 35% for all specimens in this study. Fines contents (FC) of eroded specimens under 50kPa, 100kPa, and 200kPa initial mean effective stresses are summarised in Table 5. We obtain the angles of shearing resistance (φ) at the critical state (Table 5) and the relationship between the angle of shearing resistance and fines content is fitted as a linear function (Fig. 12) with the equation shown below,

$$\varphi = a_1 \cdot FC + b_1 \tag{15}$$

where a_1=16.2, b_1=34.8. Specimens in this study are classified as coarse particles dominated soils because fines content is smaller than 35% after erosion. The angle of shearing resistance at the critical state decreases with the decrease of fines content, which is the same as the previous results (Samples 9 and 10) described above.

Here, only the fines content is considered as an explaining variable. However, as the seepage-induced erosion not only makes the fines content smaller but also makes the void ratio larger, this decrease of the angle of shearing resistance with the decrease of the fines content may have been also affected by the increase of the void ratio. Since the separation of these effects cannot be made in the experiment, the contribution of the void ratio increase cannot be explicitly expressed in this study. Presumably, the impact of the loss of fines by erosion is not large on change in the angle of shearing resistance.

4.3 Influence of erosion on the slope of the NCL (λ)

Isotropic compression tests have been conducted on both eroded and uneroded specimens, and curves of specific volume changes with mean effective stress are plotted in Fig. 13. Eroded specimen refers to the sample remaining 13% fines content after erosion under 50kPa mean stress with 35% initial fines content. The eroded specimen was firstly loaded to 100kPa, and then was unloaded down to 20 kPa. Isotropic loading was then conducted until the load reached 200 kPa, after which the eroded specimen was unloaded to 20 kPa again. At last, the isotropic compression was given to the specimen up to 300 kPa. The uneroded specimen had 35% initial fines content. The isotropic compression started from 20kPa. Firstly, the specimen was loaded to 100 kPa. Secondly, the specimen was unloaded to 20 kPa, after which the specimen was loaded to 200 kPa. Then, the specimen was unloaded to 20 kPa again. Finally, the isotropic compression was given to the specimen up to 300 kPa (see Fig. 13). By erosion, the normal compression line is shifted upward and its slope increases. However, we can observe that the swelling

line of the eroded specimen is almost parallel to that without erosion, which means that erosion has a minor effect on the slope of swelling line (Fig. 13).

Comparing to the variations of the slope of swelling line (κ) with erosion, marked change in the slope of normal compression line (λ) can be seen. Therefore, within the scope of this study, it is reasonable to ignore the erosion-indued change of κ. Based on the observation in the isotropic compression tests, we estimate the values of λ and R_0 with different fines loss from back analysis for simulation on the eroded specimens. In this paper, the increase of stiffness in small strain level for eroded specimens in the deviatoric stress-axial strain curve obtained in the experiment is ignored for simplicity. The G_0 is assumed unchanged during the simulation for both uneroded and eroded specimens based on the observation above.

4.4 Simulation of eroded specimens and evaluation of the slope of the NCL (λ)

Figure 14 shows the simulation results for the eroded specimens. Here, λ and R_0 are considered to be fitting parameters. The numerical simulation can capture the basic features of eroded specimens under the drained triaxial compression. The predicted deviatoric stress is smaller than the experimental one at the smaller strain level, which could be due to the rearrangement of soil particles after seepage test. This rearrangement would have reinforced the soil structure in the experiment. However, at the larger strain level, the predicted deviatoric stress is larger than the experimental result. It is supposed that the structure formed has been destroyed under the larger deviatoric stress, in other words, interlocking formed by clogged fines may have been broken in this stage in the experiment, but this appears less in the simulation. The predicted volumetric strains under 50kPa, 100kPa mean stresses are almost the same with the experimental ones at the larger strain level. The final axial strain under 200 kPa mean stress stops around 11%, at which the predicted volumetric strain is larger than the experimental result. However, the predicted and experimental volumetric strains under 200kPa may well be similar in the larger axial strain. When it comes to the volumetric strains under all mean stresses in the axial strain from 0-10%, all volumetric strains are overestimated. This is presumably because the Poisson's ratio is kept unchanged during the simulation. Parameters obtained from this back analysis are summarised in Table 6.

The slope of the normal compression line (λ) can be estimated with a linear empirical equation with a single soil parameter such as liquid limit for clay. For high plastic soils, as both water content and void ratio have a linear relationship with liquid limit, they can also be used for estimation of the slope of the normal compression line (Al-Khafaji & Andersland 1992). The compression of sands is mostly affected by its fabric and particle re-orientation (Sowers 1979). For both low plastic soils and high plastic sands and silts, Sower (1979) found the

linear relationship between void ratio and compression index. The similar expression will be used later to examine the relationship between the the slope of normal compression line and the void ratio before shearing.

During the process of erosion, the loss of fines may result in the larger void ratio, accompanied by the rearrangement of particles. Soil with the larger void ratio may produce larger volume change under isotropic compression. Both fines content and void ratio may have effects on the compression index. Here it is assumed that the void ratio has a greater impact on the compression index compared with fines content and the void ratio is chosen as an explaining variable in the formulation of compression index. The values of void ratio before shearing and slope of normal compression line for both uneroded and eroded specimens are summarised in Tables 3 and 6, and the relationship between the slope of normal compression line and void ratio before shearing is fitted as shown in Fig. 15 with the equation below,

$$\lambda = a_2 \cdot e_0 + b_2 \tag{16}$$

where a_2=0.045, b_2=0.028. The slope of the normal compression line increases with increasing void ratio due to erosion.

4.5 Influence of initial void ratio before shearing on the initial stress ratio

The initial stress ratio (R_0) for the eroded soil is estimated by back analysis. The overconsolidation properties of the soils can be examined by the reciprocal of the initial stress ratio. As the initial stress ratio denotes the size ratio of the initial subloading surface to the initial normal yield surface, the smaller value of initial stress ratio corresponds to the larger overconsolidation ratio or highly structured nature of the soil.

Both fines content and void ratio change with seepage. The fine particles continue decreasing and tend to be unchanged under constant flow rate. The void ratio of the soils increase gradually, during which the new arrangement is formed. Hájek et al. (2009) selected void ratio as the state variable to simulate the behaviour of soils with different over consolidation ratio. It is reasonable to select the initial void ratio to be explaining variable for the initial stress ratio in this paper. Both coarse and fine particles take part in the force chain when the fines content is around 35%. However, with increase of the void ratio, more coarse particles take part in the force chain. In this case, more pressure may act on the supporting structures (Hanna and Romhein 2008), which causes an increase in overconsolidation ratio. The interlocking prior to shearing seems stronger after erosion along with increase in the void ratio, which also makes the overconsolidation ratio larger (Mahmoudi et al. 2018). Figure.16 plots the estimated initial stress ratio against the initial void ratios before shearing for different confining pressures.

With the increase of the initial void ratio, the initial stress ratio decreases, which means the internal erosion makes the overconsolidation ratio larger or makes the soil highly structured condition.

5. Summary and conclusions

Triaxial seepage tests followed by drained compression are studied to investigate the applicability of the existing soil model to internally eroded soils. The subloading Cam-clay model is used to simulate the mechanical behaviour of eroded specimens. After confirming that the model can capture key features of uneroded specimens, the evolution of model parameters with erosion is examined by back analysis of the eroded specimens.

It is identified that the slope of the normal compression line (λ) and initial stress ratio (R_0) are the key parameters to characterise the internal erosion effects on the mechanical behaviour of the gap-graded sandy soil. Through back analysis, evolutions of the slope of normal compression line and initial stress ratio are quantified. Since the larger void ratio soil exhibits the larger volume change, the initial void ratio is selected as an explaining variable for the slope of the normal compression line and it is found that the slope of normal compression line has a positive correlation with the initial void ratio before shearing. The initial void ratio can also be explaining variable for the initial stress ratio and it is found that the initial stress ratio decreases with the increase of initial void ratio before shearing. This means that the internal erosion makes the overconsolidation ratio larger or makes the soil highly structured condition.

In the experiments, the eroded soils show a sudden change in the deviatoric stress in the smaller axial strain level (less than 1%). In the present study, this feature is ignored for simplicity. However, as this may be associated with the reinforcing effect of the clogged fines (Ke & Takahashi 2015), this effect needs further study in the future.

References

Al-Khafaji, A. W. N., & Andersland, O. B. (1992). Equations for compression index approximation. Journal of geotechnical engineering, 118(1), 148-153.

Andrianatrehina, N. L., Souli, H., Rech, J., Fry, J. J., Fleureau, J. M., & Taibi, S. (2016). Influence of the percentage of sand on the behaviobr of gap-graded cohesionless soils. Comptes Rendus Mécanique, 344(8), 539-546.

ASTM D7181-11, 2012 .Method for consolidated drained triaxial compression test for soils. Annual Book of ASTM Standards. ASTM International,West Conshohocken, PA.

Belkhatir, M., Arab, A., Della, N., Missoum, H., & Schanz, T. (2010). Influence of inter-granular void ratio on monotonic and cyclic undrained shear response of sandy soils. Comptes Rendus Mecanique, 338(5), 290-303

Bendahmane, F., Marot, D., & Alexis, A. (2008). Experimental parametric study of suffusion and backward erosion. Journal of Geotechnical and Geoenvironmental Engineering, 134(1), 57-67.

Chang, D., Zhang, L., & Cheuk, J. (2014). Mechanical consequences of internal soil erosion. HKIE Transactions, 21(4), 198-208.

Chen, C., Zhang, L. M., & Chang, D. S. (2016). Stress-Strain Behavior of Granular Soils Subjected to Internal Erosion. Journal of Geotechnical and Geoenvironmental Engineering, 142(12), 06016014.

Chien, L. K., Oh, Y. N., & Chang, C. H. (2002). Effects of fines content on liquefaction strength and dynamic settlement of reclaimed soil. Canadian Geotechnical Journal, 39(1), 254-265.

Cividini, A., Bonomi, S., Vignati, G. C., & Gioda, G. (2009). Seepage-induced erosion in granular soil and consequent settlements. International Journal of Geomechanics, 9(4), 187-194.

Fannin, R. J., & Slangen, P. (2014). On the distinct phenomena of suffusion and suffosion. Géotechnique Letters, 4(4), 289-294.

Fell, R. & Fry, J. J. (2013). State of the art on the likelihood of internal erosion of dams and levees by means of testing. In: Bonelli, S. (ed.) Erosion in Geomechanics Applied to Dams and Levees. Londan, UK: ISTE-Wiley, 1-99.

347 Ferreira, P. M. V., & Bica, A. V. D. (2006). Problems in identifying the effects of structure and critical state in a
348 soil with a transitional behaviour. Géotechnique, 56(7), 445-454.

349 Fry, J. J. (2012). Introduction to the process of internal erosion in hydraulic structures: embankment dams and
350 dikes. In: Bonelli, S. (ed.) Erosion of Geomaterials. London, UK: ISTE-Wiley, 1-36.

351 Gregory, A. S., Whalley, W. R., Watts, C. W., Bird, N. R. A., Hallett, P. D., & Whitmore, A. P. (2006). Calculation
352 of the compression index and precompression stress from soil compression test data. Soil and Tillage Research,
353 89(1), 45-57.

354 Hájek, V., Mašín, D., & Boháč, J. (2009). Capability of constitutive models to simulate soils with different OCR
355 using a single set of parameters. Computers and Geotechnics, 36(4), 655-664.

356 Hanna, A., & Al-Romhein, R. (2008). At-rest earth pressure of overconsolidated cohesionless soil. Journal of
357 geotechnical and geoenvironmental engineering, 134(3), 408-412.

358 Hashiguchi, K. (1989). Subloading surface model in unconventional plasticity. International Journal of Solids and
359 Structures, 25(8), 917-945.

360 Hicher, P. Y. (2013). Modelling the impact of particle removal on granular material behaviour. Géotechnique,
361 63(2), 118-128.

362 Ishihara, K. (1993). Liquefaction and flow failure during earthquakes. Geotechnique, 43(3), 351-451.

363 Ke, L., & Takahashi, A. (2014). Experimental investigations on suffusion characteristics and its mechanical
364 consequences on saturated cohesionless soil. Soils and Foundations, 54(4), 713-730.

365 Ke, L., & Takahashi, A. (2015). Drained monotonic responses of suffusional cohesionless soils. Journal of
366 Geotechnical & Geoenvironmental Engineering, 141(8), 1-8.

367 Lade, P. V., Liggio, C. D., & Yamamuro, J. A. (1998). Effects of non-plastic fines on minimum and maximum
368 void ratios of sand. Geotechnical Testing Journal, 21(4), 336-347.

369 Li, S., Russell, A. R., & Muir Wood, D. (2017). Stress-strain behavior of soils having undergone different
370 amounts of internal erosion. Proceedings of the 25th meeting of the Working Group on Internal Erosion in
371 embankment dams and their foundations, 114-122.

372 Mahmoudi, Y., Cherif Taiba, A., Belkhatir, M., Arab, A., & Schanz, T. (2018). Laboratory study on undrained
373 shear behaviour of overconsolidated sand–silt mixtures: effect of the fines content and stress state. International
374 Journal of Geotechnical Engineering, 12(2), 118-132.

375 Mehdizadeh, A., Disfani, M. M., Evans, R., & Arulrajah, A. (2017). Progressive Internal Erosion in a Gap-Graded
376 Internally Unstable Soil: Mechanical and Geometrical Effects. International Journal of Geomechanics, 18(3):
377 04017160

378 Muir Wood, D. & Maeda, K. (2008). Changing grading of soil: effect on critical states. Acta Geotechnica, 3(1),
379 3-14.

380 Muir Wood, D., Maeda, K., & Nukudani, E. (2010). Modelling mechanical consequences of erosion.
381 Géotechnique, 60(6), 447-457.

382 Murthy, T. G., Loukidis, D., Carraro, J. A. H., Prezzi, M., & Salgado, R. (2007). Undrained monotonic response
383 of clean and silty sands. Géotechnique, 57(3), 273-288.

384 Ni, Q., Tan, T. S., Dasari, G. R., & Hight, D. W. (2004). Contribution of fines to the compressive strength of
385 mixed soils. Géotechnique, 54(9), 561-569.

386 Ouyang, M., & Takahashi, A. (2015). Influence of initial fines content on fabric of soils subjected to internal
387 erosion. Canadian Geotechnical Journal, 53(2), 299-313.

388 Pitman, T. D., Robertson, P. K., & Sego, D. C. (1994). Influence of fines on the collapse of loose sands. Canadian
389 Geotechnical Journal, 31(5), 728-739.

390 Richart, F. E., Hall, J. R., & Woods, R. D. (1970). Vibrations of soils and foundations. Englewood Cliffs (New
391 Jersey): Prentice-Hall Inc.

392 Sowers, G. B. (1979). Introductory soil mechanics and foundations geotechnical engineering. New York, United
393 States: Macmillan Publishing Co., Inc.

394 Thevanayagam, S., Ravishankar, K., & Mohan, S. (1997). Effects of fines on monotonic undrained shear strength
395 of sandy soils. Geotechnical Testing Journal, 20(4), 394-406.

396 Wang, X., & Li, J. (2015). On the degradation of granular materials due to internal erosion. Acta Mechanica
397 Sinica, 31(5), 685-697.

Wilson, G. V., Wells, R., Kuhnle, R., Fox, G., & Nieber, J. (2018). Sediment detachment and transport processes associated with internal erosion of soil pipes. Earth Surface Processes and Landforms, 43(1), 45-63.

Yang, S., Lacasse, S., & Sandven, R. (2006). Determination of the transitional fines content of mixtures of sand and non-plastic fines. Geotechnical Testing Journal, 29(2), 102-107.

Yin, J. H. (1999). Properties and behaviour of Hong Kong marine deposits with different clay contents. Canadian Geotechnical Journal, 36(6), 1085-1095.

Zhu, H., Ye, B., Cai, Y., & Zhang, F. (2013). An elasto-viscoplastic model for soft rock around tunnels considering overconsolidation and structure effects. Computers and Geotechnics, 50, 6-16.

Zuo, L., & Baudet, B. A. (2015). Determination of the transitional fines content of sand-non plastic fines mixtures. Soils and Foundations, 55(1), 213-219.

Table 1 Property of silica sands

Property	Silica No.3	Silica No.8
Specific gravity	2.63	2.63
Median particle size (mm)	1.72	0.16
Effective particle size (mm)	1.37	0.087
Maximum void ratio	1.009	1.333
Minimum void ratio	0.697	0.703

Table 2 Details of particle sizes, curvature coefficient and uniformity coefficient

Specimens	D_{10}	D_{30}	D_{60}	C_u	C_c
35 N50	0.10	0.21	1.73	17.3	0.25
35 E50	1.15	1.60	1.88	1.63	1.18
35 E100	0.21	1.55	1.88	8.95	6.09
35 E200	0.10	1.28	2.02	20.2	8.11

Note: Specimens named with"35" refer to the initial fines content is 35%. "50, 100, 200" indicate the initial mean stress, 50kPa, 100kPa, 200kPa respectively. "E" means eroded specimens, while "N" represents sample without erosion.

Table 3 Parameters for specimens without erosion

Specimens	λ	κ	M	R_0	e_0
35N-50	0.052	0.014	1.65	0.71	0.55
35N-100	0.052	0.014	1.65	1.0	0.56
35N-200	0.052	0.014	1.65	1.0	0.54

Table 4 Influence of fines content on shear strength

Sample	Drained/ Undrained	Ranges of fines content	Types of fines	Positive/Negative Correlation	Reference
1	Undrained	3%-18%	Plastic	Negative	Ishihara 1993
2	Undrained	10%-40%	Plastic	Negative	Pitman et al. 1994
2'	Undrianed	0%-40%	Non-plastic	Positive	Pitman et al. 1994
3	Undrained	12%-27%	Non-plastic	Negative	Thevanayagam et al. 1997
4	Undrained	6%-27.5%	Plastic	Negative	Yin 1999
5	Undrained	0%-30%	Non-plastic	Negative	Chien et al. 2002
6	Undrained	0%-20%	Non-plastic	Positive	Ni et al. 2004
6'	Undrained	0%-20%	Plastic	Negative	Ni et al. 2004
7	Undrained	0%-15%	Non-plastic	Positive	Murthy et al. 2007
8	Undrained	0%-50%	Non-plastic	Negative	Belkhatir et al. 2010
9	Drained	25%-35%	Non-plastic	Positive	Chang et al. 2014
10	Drained	5%-35%	Non-plastic	Positive	Chen et al. 2016

Table 5 Influence of fines content on angle of shearing resistance

Specimens	FC (%)	φ (°)
35N*	35.0	40.3
35E200	24.6	37.6
35E100	15.5	37.1
35E50	13.1	36.2

Note: 35N* denotes uneroded specimens with 35% initial fines content under 50kPa, 100kPa and 200kPa mean stresses.

Table 6 Parameters for specimens with erosion

Specimens	λ	M	R_0	e_0	FC (%)
35 E50	0.072	1.47	0.67	1.01	13.1
35 E100	0.069	1.51	0.83	0.92	15.5
35 E200	0.064	1.53	0.94	0.77	24.6

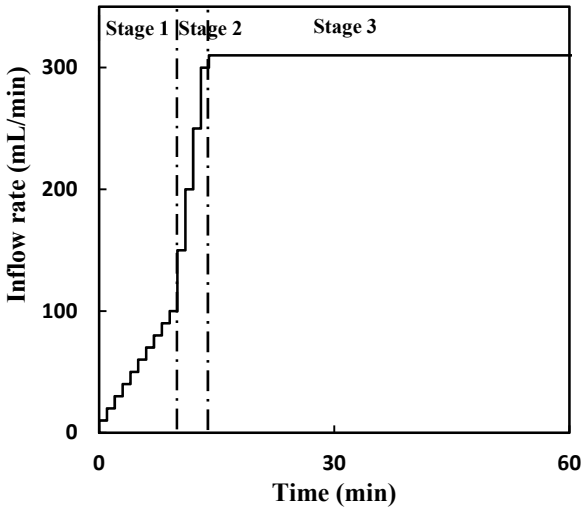

Fig.1 Inflow rate for seepage test

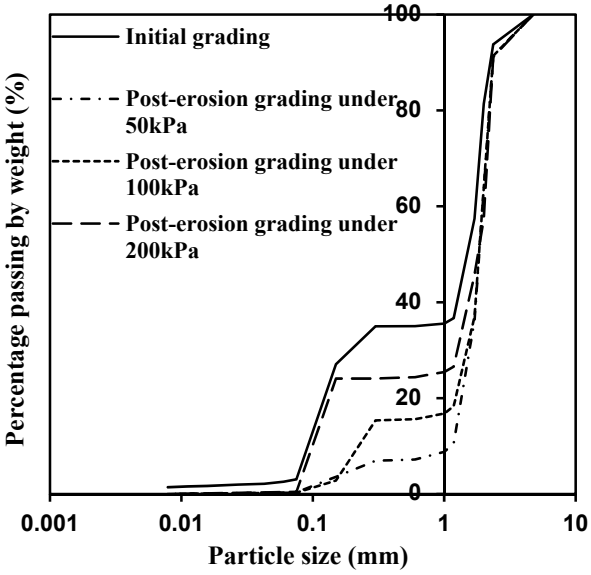

Fig. 2 Particle size distribution curves before and after erosion

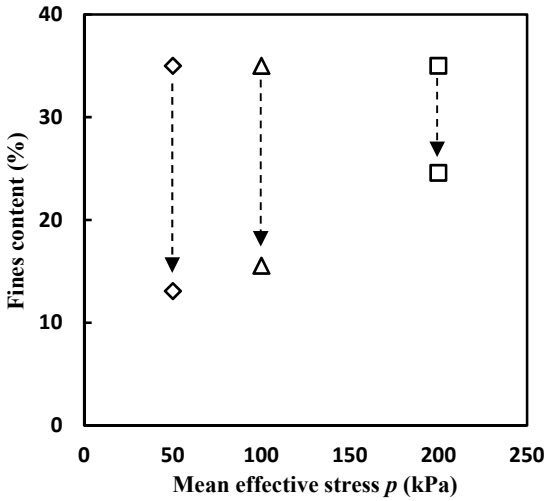

Fig. 3 Erosion-induced change of fines content for different initial mean effective stress

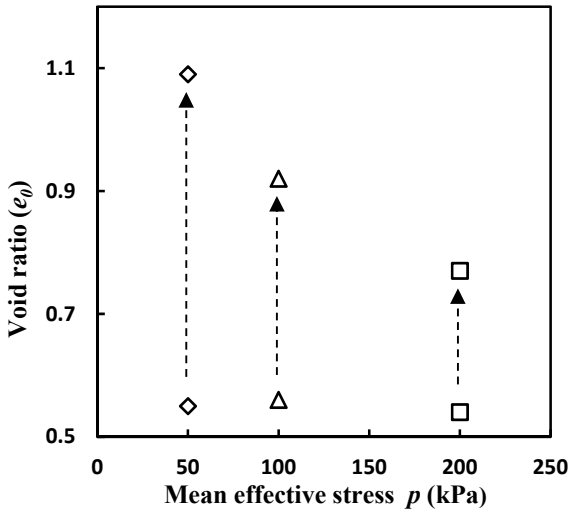

Fig. 4 Erosion-induced change of void ratio for different initial effective confining stresses

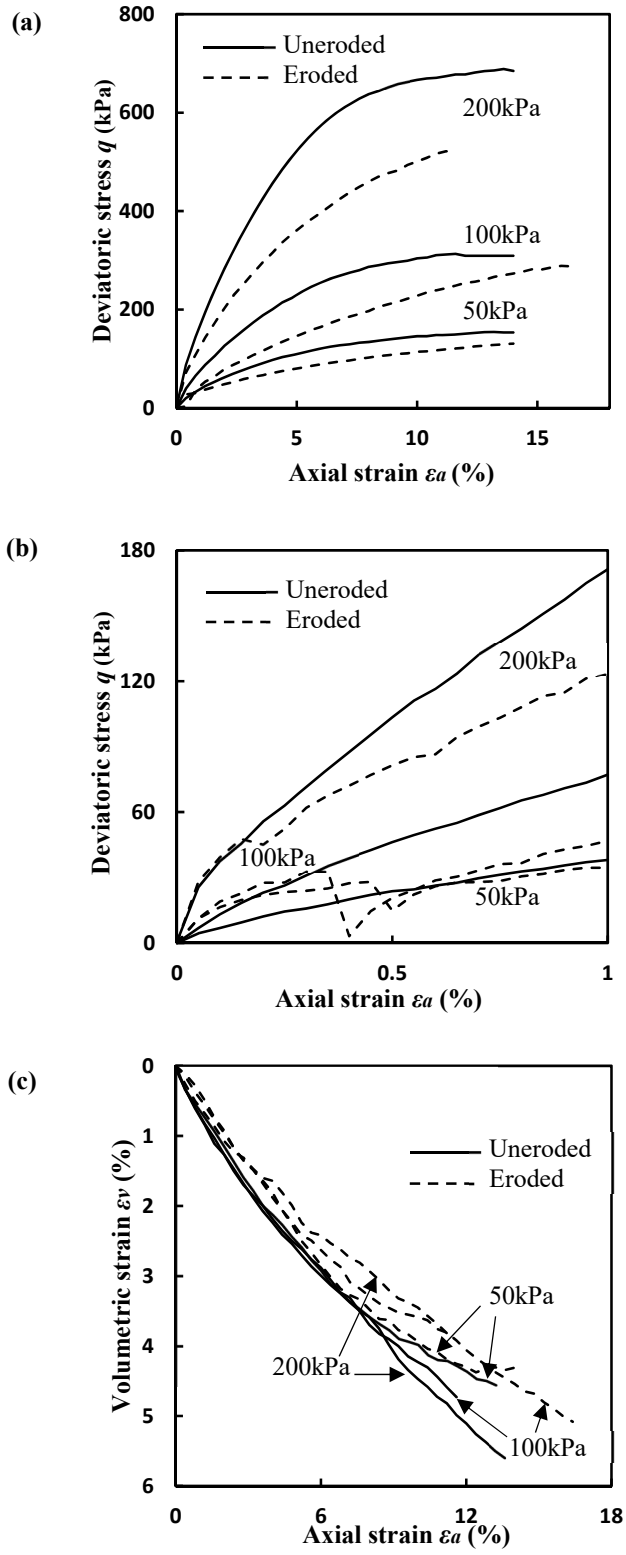

Fig. 5 Mechanical behaviour of both uneroded and eroded specimens under drained triaxial compression tests. **a** deviatoric stress-axial strain relationships, **b** deviatoric stress-axial strain relationships with axial strain smaller than 1%, **c** volumetric strain-axial strain relationships

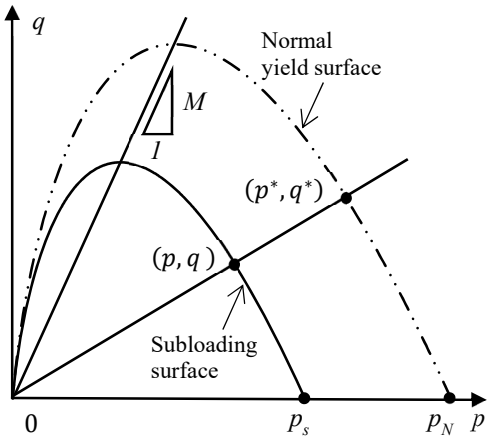

Fig. 6 Subloading surface and normal yield surface

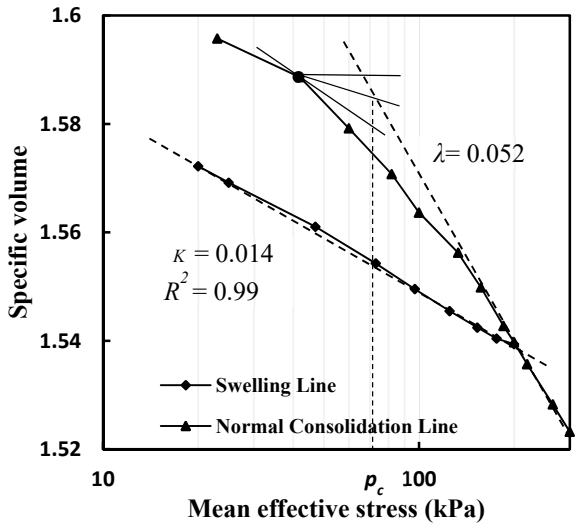

Fig. 7 Isotropic volume change of uneroded specimen

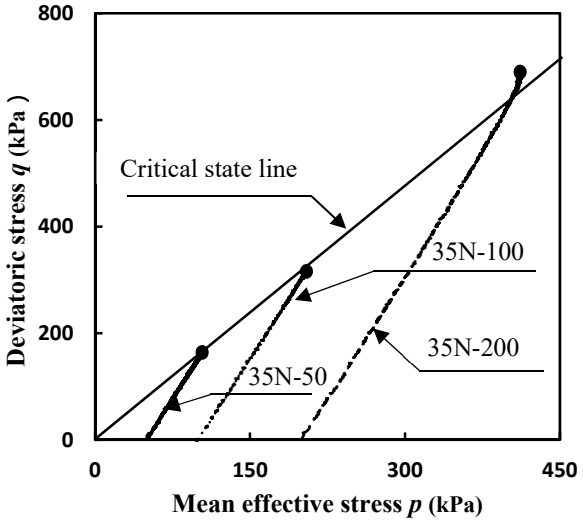

Fig. 8 Effective stress paths in drained triaxial tests on uneroded specimens

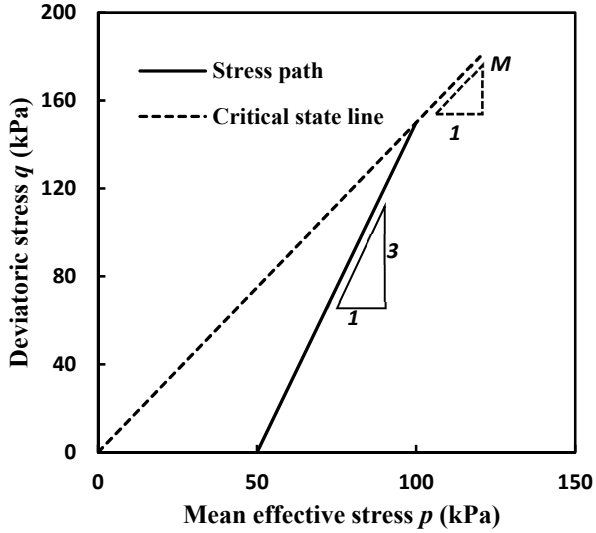

Fig. 9 Critical state line and stress path in *p*-*q* space

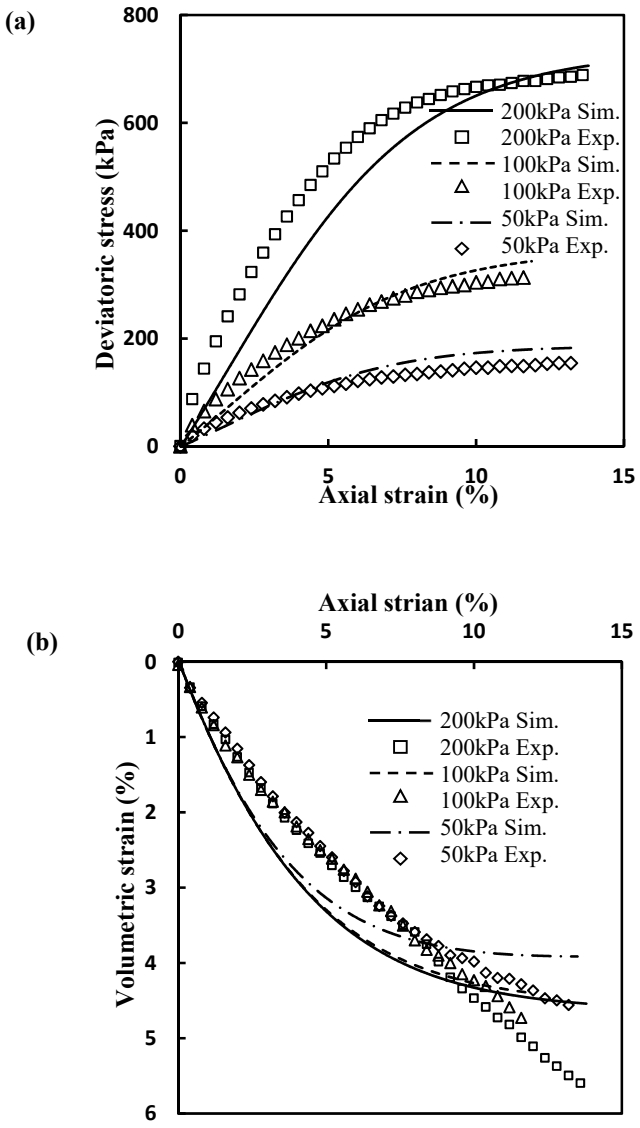

Fig. 10 Predictions of mechanical behaviour of uneroded specimens under triaxial compression, **a** stress-strain response, **b** volumetric strain-axial strain response

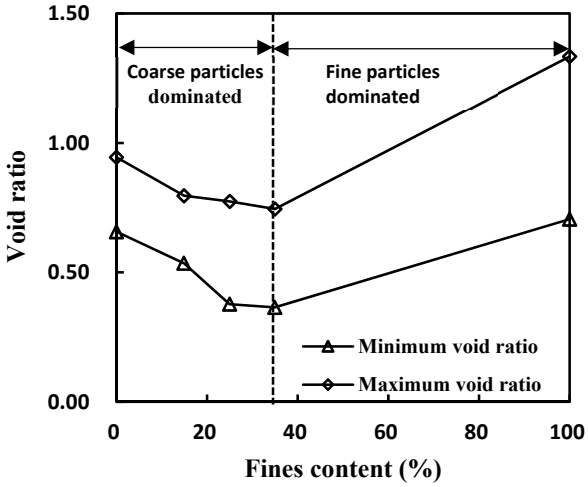

Fig. 11 Change of maximum and minimum void ratios with fines content

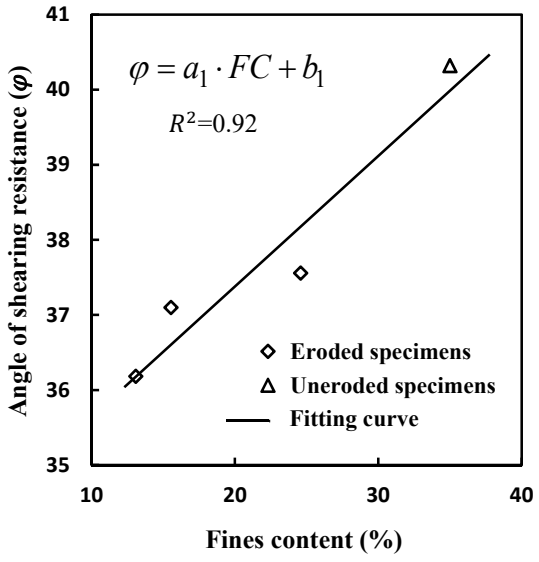

Fig. 12 Angle of shearing resistance versus fines content

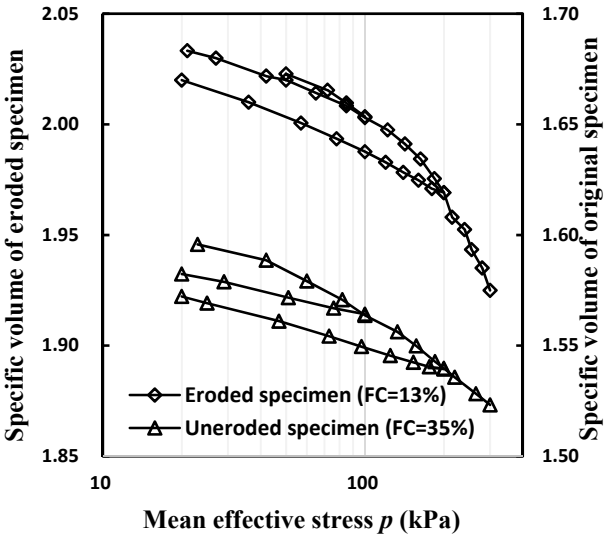

Fig. 13 Normal compression lines and swelling lines for eroded and uneroded specimens

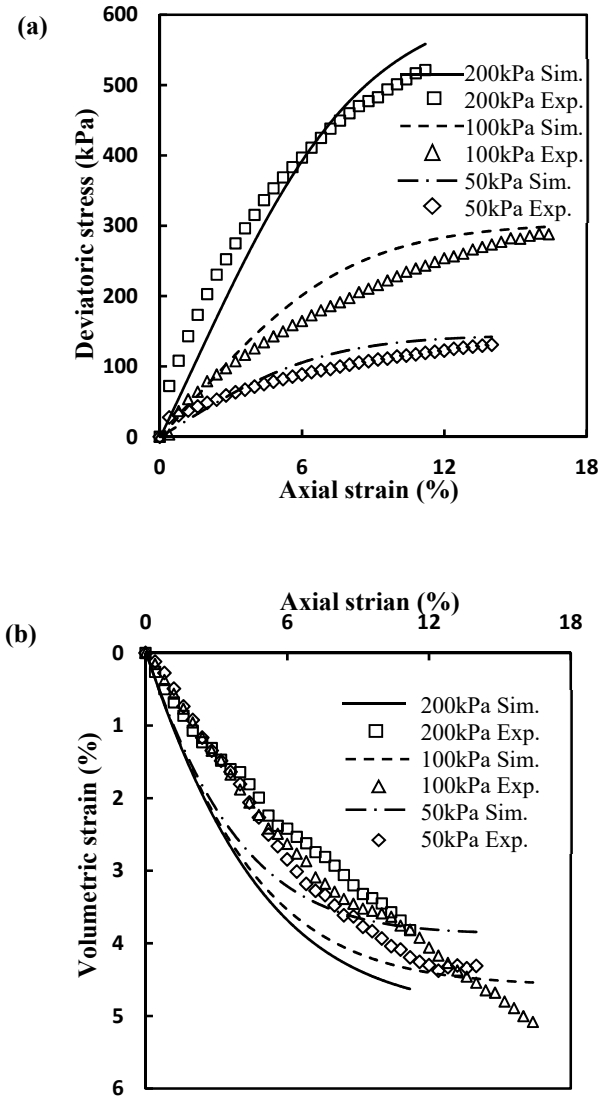

Fig. 14. Predictions of mechanical behaviour of eroded specimens under triaxial compression. **a** stress-strain response, **b** volumetric strain-axial strain response

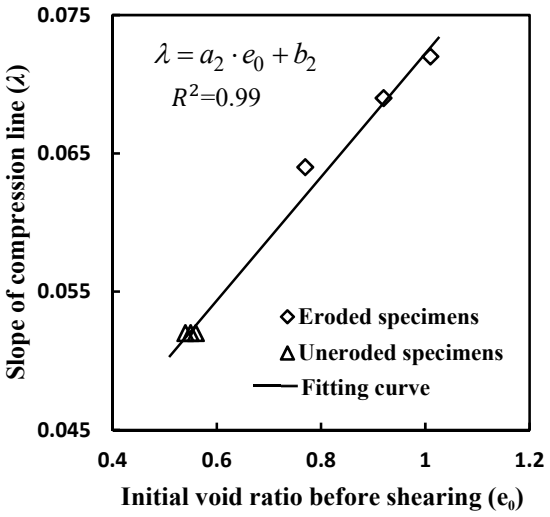

Fig. 15 Change in slope of normal compression line with initial void ratio before shearing

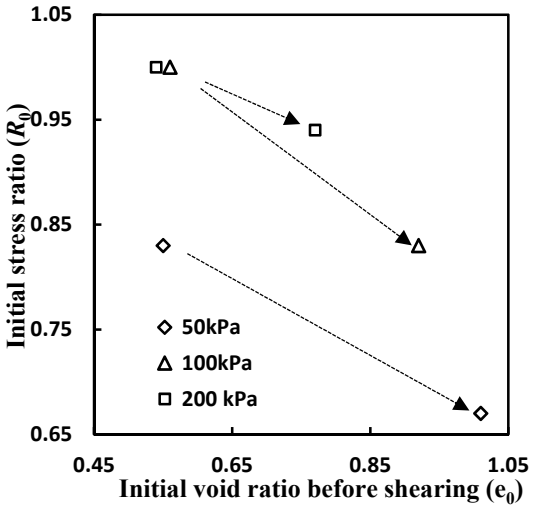

Fig. 16 Estimated initial stress ratio against initial void ratio before shearing